

Modeling and Optimization of HAZ Characteristics for Submerged Arc Welded High Strength Pipeline Steel

Satish Kumar Sharma¹  · Sachin Maheshwari² · Ratnesh Kumar Raj Singh¹

Received: 17 January 2018 / Accepted: 5 November 2018 / Published online: 6 December 2018
© The Indian Institute of Metals - IIM 2018

Abstract Heat affected zone (HAZ) is the most critical part of welded pipe in oil and gas pipelines as HAZ shows more susceptibility toward embrittlement and weld cracking. It happens because microstructural changes occur due to high heat of welding. Heat input and preheating temperature together control the cooling time of weld which in turn determines the weld microstructure and its mechanical properties. Therefore, in the present study, effect of heat input as well as preheating temperature on the characteristics of the HAZ in submerged arc-welded high-strength low alloy (HSLA) pipeline steel was studied. Hardness and area of HAZ were observed and analyzed as HAZ characteristics. Heat input of the process was varied by changing the voltage, welding speed, wire feed rate and contact tube to work distance. Experiments were designed using central composite rotatable design (CCRD) approach, and using response surface methodology (RSM), process modeling was done. For the purpose of single- as well as multi-characteristic optimization, desirability approach was used. Relationship of heat input and critical cooling rate with HAZ characteristics and its microstructure was also revealed. Inclusion of preheating temperature

led to significant improvement in the HAZ characteristics of the weld.

Keywords Heat input · Cooling time · Heat affected zone · Desirability · Submerged arc welding · Optimization

1 Introduction

Owing to its excellent mechanical properties at low temperature, API X80 is the first choice for today's need of high-pressure pipeline in oil and gas industry [1]. This steel with minimum yield strength of 555 MPa comes under the category of HSLA steels [2]. In pipeline industry, X80 steel is suitable for both offshore as well as onshore applications at high pressure. Out of API grade steels used for fabrication of oil and gas pipelines, X80 steel is preferred over all others because of its high strength to weight ratio and very fine grain structure which shows high impact strength at low temperatures. In welding of these high-strength pipeline steels, submerged arc welding (SAW) operation is the most preferred joining technique. In pipeline fabrication industry, SAW is also advantageous because of its ability to produce sound quality welded joint with high material deposition rate [3]. The welded structures of high-strength materials used in pipeline or pressure vessels have to withstand the severe conditions of operational environment [4]. In welds produced using high heat input processes like SAW, its HAZ is the most critical part as it shows more susceptibility toward embrittlement and weld cracking [5]. Therefore, for a long-life welded joint in pipes and/or pipelines, minimum HAZ area is favorable. HAZ area is a measure of the extent of the thermal cycle effect on parent material during welding operation [6, 7]. Moreover, it is the thermal effect of welding heat which

✉ Satish Kumar Sharma
satishsharma847@gmail.com

Sachin Maheshwari
ssaacchhiinn@gmail.com

Ratnesh Kumar Raj Singh
rkrs73@gmail.com

¹ Mechanical Engineering Department, Thapar Institute of Engineering and Technology, Patiala, Punjab 147004, India

² Division of Manufacturing Processes and Automation Engineering, Netaji Subhas University of Technology, Dwarka, New Delhi 110078, India

alters the microstructure in HAZ from parent one to a crack susceptible structure [8]. Generally, in field welding, an idea about material's microstructure and its behavior during service is taken from its hardness value. Hardness index also provides an idea about its susceptibility towards hydrogen-assisted cold cracking. A higher hardness value gives an indication of brittle structure which is more prone to failure during service [5]. Similarly, hardness test provides numerical values which may be used for comparison and analysis purpose during selection and formulation of welding procedures. Results of hardness tests can also be utilized while diagnosing the causes of weld failure [9].

Both of these HAZ characteristics (HAZ area and its hardness) signify the severity of the effect of welding heat on parent material in weld proximity of the joint. For a better quality welded joint, minimum area and minimum hardness of HAZ are desired which are the functions of cooling rate [10]. Heat input and preheating temperature together control the cooling time of HAZ which in turn determines its microstructure and mechanical properties. The studies reported in the literature specifically in the field of pipe and pipeline fabrication industry have investigated the HAZ characteristics at different welding heat inputs by conducting laboratory or field experiments for various industry-relevant welding operations such as SAW [11–13], double-wire tandem SAW [14], gas metal arc welding [15], gas tungsten arc welding [16] and manual metal arc welding [17]. In these studies, preheating temperature and/or interpass temperature between welding passes is not given due consideration while investigating the HAZ and its characteristics.

In last few decades, thermo-physical simulation approach is used to investigate welding HAZ characteristics. Approach of simulated HAZ investigation to predict the behavior of real welding HAZ is widely applied by many researchers of pipe and pipeline fabrication industry [18–23] as it provides the opportunity to control the cooling rate in large volume of HAZ. However, the laboratory conditions and its controlled environment of simulation are far away from the practical situation of real field welding applied in pipe and pipeline fabrication. Therefore, there is need to fill this gap through experimentation of producing real welding HAZ with different cooling rates for most popularly used SAW operation on high-strength steel and then investigation of HAZ characteristics which can be successfully used by the welders of oil and gas pipeline industry.

Keeping this in view, two characteristics of welding HAZ: HAZ area and HAZ hardness, are investigated and modeled for a real weld through CCRD design approach of RSM. Along with heat input varying parameters, preheating temperature has also been considered as a process variable. Main as well as interaction effects of all variables

are presented and further discussed. As critical cooling time of a weld depends upon the heat input and preheating temperature, critical cooling time is also calculated for each weld. Moreover, the relationship of both HAZ characteristics with heat input and critical cooling time has also been explored along with its microstructural investigation.

2 Materials and methods

2.1 Material details

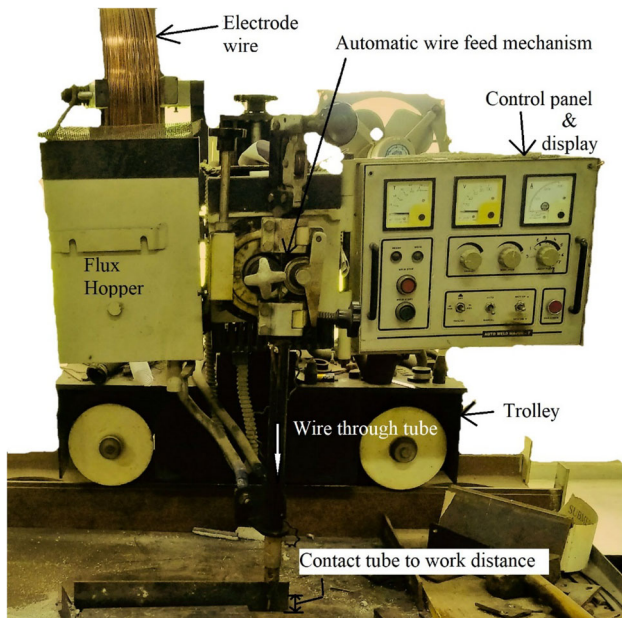
In the present study, API X80 steel plates were used having dimensions of 300 mm x 150 mm x 24 mm as base material. Consumables like flux and electrode wire, were selected as per AWS-A5.23:EF3EG specification. The filler wire of 4 mm diameter (trade name OE-SD31Ni1/2Mo) and flux of fluoride base with basicity index 3.1 prepared through agglomeration (trade name OP121TT/W) were used. Chemical composition in weight percentage of elements for HSLA-X80 steel and filler wire is listed in Table 1.

2.2 Welding procedure

Using SAW operation, bead-on-plate experiments were performed on the flat surfaces of API-X80 steel plates. For that purpose, a constant-voltage-type DC power source was used in this study. Before welding, plate surfaces used to deposit weld beads were carefully cleaned. Electric furnace was used to preheat each plate. For uniform heating of the whole plate up to required preheating temperature, heating time was kept as 1 h. Electric furnace was kept near to the SAW machine in the same laboratory to minimize the heat loss. In submerged arc welding process, DC electrode positive polarity is better for maximum penetration or dilution with the best bead shape and resistance to porosity; therefore, the same has been used in this study. Figure 1 shows the welding trolley with attached control panel and nozzle with electrode wire feeding mechanism. Selection of welding parameters and their range was done while giving proper consideration to heat input and cooling rate of weld. Heat input and preheating temperature together controlled the cooling rate of weld which finally decided the extent of parent material which got affected due to heat, i.e., HAZ area and alteration in its microstructure and hence mechanical properties like hardness. As per the established literature, voltage, welding speed, wire feed rate and contact tube to work distance control the welding heat input while preheating temperature affects the cooling time of the weld along with heat input. To avoid any systematic error in the process, experiments were carried

Table 1 Chemical composition of API X80 steel and consumable electrode wire

Element	Fe	C	Si	Mn	S	P	Ni	Cr	Mo
API X80	97.39	0.053	0.225	1.59	0.005	0.0095	0.189	0.103	0.259
Electrode wire	96.37	0.13	0.22	1.73	0.004	0.007	0.93	0.03	0.53
Element	Al	Cu	Ti	Nb	Co	V	Pb	Zr	B
API X80	0.036	0.057	0.018	0.036	< 0.01	0.018	< 0.01	< 0.006	< 0.0005
Electrode wire	0.002	0.04	–	–	–	0.01	–	–	–

**Fig. 1** SAW trolley with control panel, wire feed mechanism, contact tube and flux hopper

out at random. As process responses, HAZ area and HAZ hardness were measured.

2.3 Response measurement

A weld bead on the surface of the plate was deposited for each setting of designed experiment. From these bead-on-plate welds, a small piece, for measurement of bead geometry parameters, was cut in such a way that the weld lied in the centre. Cutting of weld pieces was carried out using abrasive cutter with continuous supply of coolant. This cut surface of the piece was polished with emery papers of different grades starting from 100 through 1200 number of SiC abrasive followed by super-polishing. To reveal the bead geometry parameters, 5% concentrated Nital solution was applied on the exquisitely polished surface. The geometry revealed after etching, typically for weld number 17, is clearly depicted in Fig. 2a.

HAZ area was measured with the help of a stereo-zoom microscope by selecting the enclosed area clearly visible

after etching of the polished surface. Hardness of HAZ was measured using Vickers hardness tester and expressed as Vicker hardness number (VHN). Hardness profile was measured in the transverse piece of welded joint which includes weldment, HAZ and base metal as shown in the schematic sketch (refer Fig. 2b). Hardness profile was measured from weld centre to unaffected base metal in the middle of the weld.

2.4 Calculation of heat input and critical cooling time

Heat input value for each experiment was determined using Eq. 1 considering thermal efficiency of welding arc as 0.85 [24]. Average value of welding current and arc voltage were determined by collecting the V-I transient data. For that purpose, a data acquisition system was incorporated with the power source. Critical cooling time duration (time taken by weld to cool down from 800 to 500 °C) denoted by $\Delta t_{8/5}$ was calculated using Eq. 2 [25].

$$\text{Heat input} = \eta \frac{V \times I \times 60}{N \times 1000} \text{ (kJ/mm)}, \quad (1)$$

where η = thermal efficiency of welding arc, I = welding current (A), V = arc voltage (V), N = welding speed (mm/min).

$$\Delta t_{8/5} = \frac{\text{Heat input}}{2\pi k} \cdot \left[\frac{1}{500 - T_0} - \frac{1}{800 - T_0} \right] \text{ (s)}, \quad (2)$$

where k = thermal conductivity (taken as 50 J/s.m. °C for steel) and T_0 = initial or preheating temperature in °C (taken as 30 °C).

2.5 Response surface methodology (RSM)

RSM may be considered as an aggregation of some statistical and mathematical techniques. RSM is used to optimize a response through process modeling and analysis where it is influenced by many process variables [26]. For simple cases, it is preferred to apply a first order or linear model to find an approximate relationship between process variables and their response. But for detailed analysis,

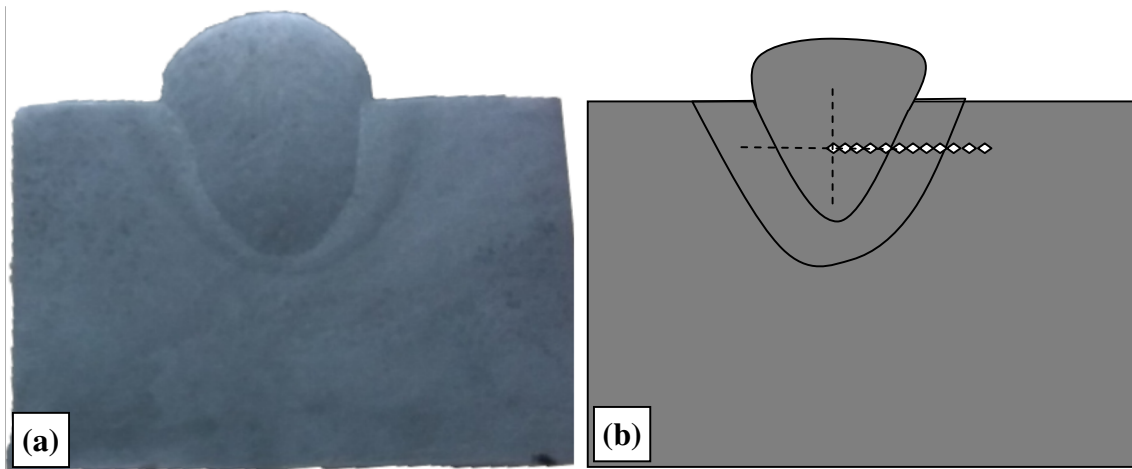


Fig. 2 **a** Macrograph of cross-sectional cut part with revealed bead geometry and **b** schematic diagram showing HAZ area and hardiness measurement pattern

second-order model (Eq. 3) is recommended as it takes into consideration the interaction effect amid process variables and surface curvature [27]:

$$f = \beta_0 + \sum_{i=1}^k \beta_i x_i + \sum_{i=1}^k \beta_{ii} x_i^2 + \sum_{i < j} \beta_{ij} x_i x_j + \varepsilon, \quad (3)$$

where f = process response, x_i = process variables, k = number of process variables, β_i = regression coefficient and ε = value of error observed in process response.

Converting the actual values of different responses into coded values bring the variables in the same order of magnitude. Therefore, this conversion makes the regression analysis more fruitful. Each process parameter is varied at five levels over its working range. This conversion has been carried out using Eq. 4 [26]:

$$\text{Coded value} = \frac{2[\text{Actual value} - (\text{Maximum value} + \text{Minimum value})]}{(\text{Maximum value} - \text{Minimum value})} \quad (4)$$

Settings of process parameters (listed in Table 2) for each experiment designed according to CCRD approach are tabulated in Table 3 along with results obtained of HAZ characteristics in corresponding weld.

2.6 Desirability function

A multiple response optimization technique called desirability function was demonstrated by Derringer and Suich. According to the approach of desirability function technique, an individual desirability function (d_i) value is assigned to each process response $f_i(x)$ in the range of 0 to 1. Depending on the type of response characteristics,

desirability function can be of three types (Eqs. 5, 6 and 7) [28].

$$d_i = \begin{cases} 0, & f_i \leq f_{i*} \\ \left(\frac{f_i - f_{i*}}{f_i' - f_{i*}} \right)^r, & f_{i*} < f_i < f_i' \\ 1, & f_i \geq f_i' \end{cases} \quad (5)$$

where f_{i*} = minimum acceptable value of f_i , f_i' = highest value of f_i and r = shape function for desirability.

$$d_i = \begin{cases} 1, & f_i \leq f_i'' \\ \left(\frac{f_i'' - f_i}{f_i'' - f_i^*} \right)^s, & f_i'' < f_i < f_i^* \\ 0, & f_i \geq f_i^* \end{cases} \quad (6)$$

where f_i'' = lowest value of f_i and f_i^* = maximum acceptable value of f_i and s = shape function for desirability.

$$d_i = \begin{cases} \left(\frac{f_i - f_i^*}{T_i - f_i^*} \right)^p, & f_i^* < f_i < T_i \\ \left(\frac{f_i - f_i^*}{T_i - f_i^*} \right)^q, & T_i < f_i < f_i^* \\ 0, & f_i > f_i^* \text{ or } f_i^* > f_i \end{cases} \quad (7)$$

where T_i = target value, p and q = exponential parameters that decide the shape of desirability function.

For each experiment, individual desirability function values of all responses are combined and converted into a single value called overall desirability function (D) of the process. It can be represented as $D = (d_1^{w_1} \cdot d_2^{w_2} \cdot \dots \cdot d_n^{w_n})$, where w_j is the weightage assigned to the j th response as per its importance. It should also satisfy the condition as $\sum_{j=1}^n w_j = 1$.

In the present study, $r = s = 1$ has been considered. The parameter settings which yielded maximum value of overall desirability function value have been considered as

Table 2 Process parameters and their levels used for this study

Process parameters	Notation	Units	Levels				
			- 2	- 1	0	+1	+2
Open-circuit voltage	<i>A</i>	Volt	30	32	34	36	38
Welding speed	<i>B</i>	cm/min	25	30	35	40	45
Contact tube to workpiece distance	<i>C</i>	mm	24	28	32	36	40
preheating temperature	<i>D</i>	°C	60	120	180	240	300
Wire feed rate	<i>E</i>	mm/s	20	25	30	35	40

Table 3 Central composite rotatable designed experiment settings with results

Run No.	Std No.	Process parameters in coded values					Process parameters in actual values					$\Delta t_{8/5}$ (s)	Heat input (kJ/mm)	HAZ area (mm ²)	HAZ hardness (VHN)
		A	B	C	D	E	A	B	C	D	E				
1	12	1	1	- 1	1	- 1	36	40	28	240	25	13.86	2.11	80.71	220
2	26	0	0	0	0	2	34	35	32	180	40	13.38	2.78	91.58	209
3	28	0	0	0	0	0	34	35	32	180	30	12.32	2.56	78.55	218
4	11	- 1	1	- 1	1	1	32	40	28	240	35	14.20	2.17	75.22	219
5	16	1	1	- 1	1	1	36	40	36	240	35	15.43	2.35	108.76	214
6	01	- 1	- 1	- 1	- 1	1	32	30	28	120	35	10.96	2.97	86.44	222.5
7	32	0	0	0	0	0	34	35	32	180	30	12.20	2.53	88	226
8	03	- 1	1	- 1	- 1	- 1	32	40	28	120	25	7.10	1.92	60.09	228
9	30	0	0	0	0	0	34	35	32	180	30	12.22	2.53	85.83	217
10	10	1	- 1	- 1	1	1	36	30	28	240	35	20.72	3.15	130.35	206
11	14	1	- 1	1	1	- 1	36	30	36	240	25	17.73	2.70	137.25	203
12	17	- 2	0	0	0	0	30	35	32	180	30	9.81	2.04	54.11	221
13	20	0	2	0	0	0	34	45	32	180	30	8.71	1.81	65.73	237
14	08	1	1	1	- 1	- 1	36	40	36	120	25	7.37	2.00	60.8	211
15	19	0	- 2	0	0	0	34	25	32	180	30	15.38	3.20	126.22	218
16	31	0	0	0	0	0	34	35	32	180	30	12.20	2.53	83	218
17	24	0	0	0	2	0	34	35	32	300	30	22.26	2.33	106.83	203
18	27	0	0	0	0	0	34	35	32	180	30	12.20	2.53	86	220
19	15	- 1	1	1	1	- 1	32	40	36	240	25	11.95	1.82	73.06	217.3
20	02	1	- 1	- 1	- 1	- 1	36	30	28	120	25	10.31	2.79	84.51	221
21	23	0	0	0	- 2	0	34	35	32	60	30	6.94	2.36	70.07	228
22	06	1	- 1	1	- 1	1	36	30	36	120	35	9.11	2.47	105.95	213.3
23	13	- 1	- 1	1	1	1	32	30	36	240	35	17.09	2.60	92	218
24	22	0	0	2	0	0	34	35	40	180	30	11.14	2.31	83.62	207.3
25	07	- 1	1	1	- 1	1	32	40	36	120	35	7.49	2.02	64.37	223
26	09	- 1	- 1	- 1	1	- 1	32	30	28	240	25	16.48	2.51	90.21	225.3
27	29	0	0	0	0	0	34	35	32	180	30	12.20	2.53	85	221
28	05	- 1	- 1	1	- 1	- 1	32	30	36	120	25	8.90	2.41	94.91	210
29	25	0	0	0	0	- 2	34	35	32	180	20	9.46	1.96	74.16	206
30	21	0	0	- 2	0	0	34	35	24	180	30	11.36	2.35	68.99	221
31	18	2	0	0	0	0	38	35	32	180	30	12.77	2.65	97.38	208
32	4	1	1	- 1	- 1	1	36	40	28	120	35	8.88	2.40	77.12	219.3

optimal. Goal of the present study is to find optimal parameter setting that maximizes the overall desirability

function value individually for minimum HAZ area and minimum HAZ hardness and simultaneously for both.

3 Results and discussion

3.1 ANOVA analysis and mathematical modeling

From the experimental result for HAZ area and its hardness (Table 3), the regression coefficients for a second-order polynomial regression model have been determined for each at 95% confidence level. Along with significance test for regression model and its coefficients, ANOVA analysis has been carried out to be sure about model's accuracy. In addition to goodness-of-fit test, test for lack-of-fit and adequacy check are also conducted for the developed model.

Depending on the results of the fit summary analysis, quadratic models are found to be statistically significant and non-aliased. In Tables 4 and 5, details of ANOVA analysis for the quadratic model and its terms are tabulated for the HAZ area and HAZ hardness, respectively. A large *F* value for both models implies that both models are significant. Nonsignificant terms are eliminated from the model using backward elimination. For a model to be fit to represent the response outcome for those settings of process variables at which experiments are not performed, its lack-of-fit test should be nonsignificant. For both models, lack-of-fit is found to be nonsignificant while relating it to the pure error.

R^2 values of models for HAZ area and HAZ hardness are 0.97 and 0.81, respectively. Both values are very close to unity. It means that 97% and 81% of variations can be explained by these models, respectively. It indicates high accuracy of both the models. The predicted R^2 value of 0.9079 is in close proximity to Adj R^2 value of 0.9477 which is desirable for a well-fitted model. Figures 3a and 4a show the normal probability plots of residuals for HAZ area and HAZ hardness, respectively. It shows that the residuals are spread around the straight line. It happens in case of normal distribution of error which is always desirable for a good quality model. In Figs. 3b and 4b, predicted values of the quadratic regression model are plotted against the actual experimental values. It clearly expresses that actual values are in good agreement with predicted values of the responses within the working limits of process variables. The adequate precision of a model is calculated to understand the relationship between the desired and undesired responses, i.e. signal-to-noise ratio. For a good quality model, a higher value of adequate precision is always desirable. For both models, sufficiently large adequate precision value indicates that its signal-to-noise ratio is significant.

As a result of multiple regression analysis on the results of HAZ area and HAZ hardness, quadratic equations are obtained in coded as well as actual factors as shown in Eqs. 8 and 9 and Eqs. 10 and 11, respectively.

Table 4 ANOVA for response surface reduced quadratic model of HAZ area

Source	Sum of squares	Degree of freedom	Mean square	<i>F</i> Value	<i>p</i> value	
Model	11810.28	12	984.19	47.81	< 0.0001	Significant
A	2314.57	1	2314.57	112.44	< 0.0001	
B	4886.9	1	4886.9	237.41	< 0.0001	
C	278.19	1	278.19	13.51	0.0016	
D	2144.96	1	2144.96	104.2	< 0.0001	
E	364.34	1	364.34	17.7	0.0005	
AB	99.25	1	99.25	4.82	0.0407	
AD	676.13	1	676.13	32.85	< 0.0001	
AE	218.67	1	218.67	10.62	0.0041	
BE	115.29	1	115.29	5.6	0.0287	
CE	147.32	1	147.32	7.16	0.015	
B ²	466.61	1	466.61	22.67	0.0001	
D ²	128.14	1	128.14	6.23	0.022	
Residual	391.11	19	20.58			
Lack-of-fit	337	14	24.07	2.22	0.1933	Not significant
Pure error	54.11	5	10.82			
Cor total	12201.39	31				
SD	4.54		<i>R</i> -squared	0.97		
Mean	86.46		Adj <i>R</i> -squared	0.95		
C.V. %	5.25		Pred <i>R</i> -squared	0.91		
PRESS	1123.89		Adeq precision	27.99		

Table 5 ANOVA for response surface reduced quadratic model of HAZ hardness

Source	Sum of squares	Degree of freedom	Mean square	F value	<i>p</i> value prob > F	
Model	1567.73	8	195.97	12.32	< 0.0001	Significant
A	276.76	1	276.76	17.40	0.0004	
B	207.09	1	207.09	13.02	0.0015	
C	259.38	1	259.38	16.31	0.0005	
D	237.51	1	237.51	14.93	0.0008	
E	1.26	1	1.26	0.08	0.7808	
CE	185.64	1	185.64	11.67	0.0024	
B ²	181.11	1	181.11	11.39	0.0026	
E ²	192.31	1	192.31	12.09	0.002	
Residual	365.79	23	15.90			
Lack-of-fit	311.79	18	17.32	1.60	0.3161	Not significant
Pure error	54.00	5	10.80			
Cor total	1933.52	31				
SD	3.99		<i>R</i> -squared	0.81		
Mean	217.16		Adj <i>R</i> -squared	0.75		
C.V. %	1.84		Pred <i>R</i> -squared	0.63		
PRESS	716.29		Adeq Precision	15.29		

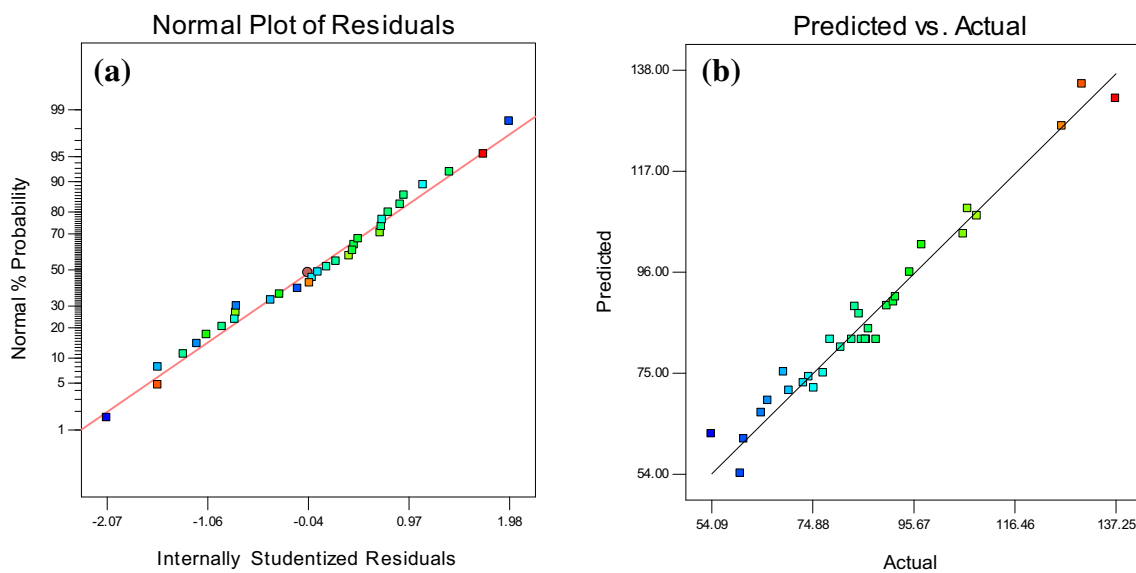


Fig. 3 **a** Normal probability plot of residuals and **b** plot of predicted response vs. actual value for HAZ area

Quadratic model for HAZ characteristics in terms of coded values of process parameters:

$$\begin{aligned}
 \text{HAZ Area} = & 81.95 + 9.82 * A - 14.27 * B + 3.40 * C \\
 & + 9.45 * D + 3.90 * E - 2.49 * A * B \\
 & + 6.50 * A * D + 3.70 * A * E + 2.68 * B \\
 & * E - 3.03 * C * E + 3.95 * B^2 + 2.07 \\
 & * D^2
 \end{aligned}$$

(8)

$$\begin{aligned}
 \text{HAZ Hardness} = & +217.21 - 3.40 * A + 2.94 * B \\
 & - 3.29 * C - 3.15 * D + 0.23 * E \\
 & + 3.41 * C * E + 2.46 * B^2 - 2.54 \\
 & * E^2
 \end{aligned}$$

(9)

Quadratic model for HAZ characteristics in terms of actual values of process parameters:

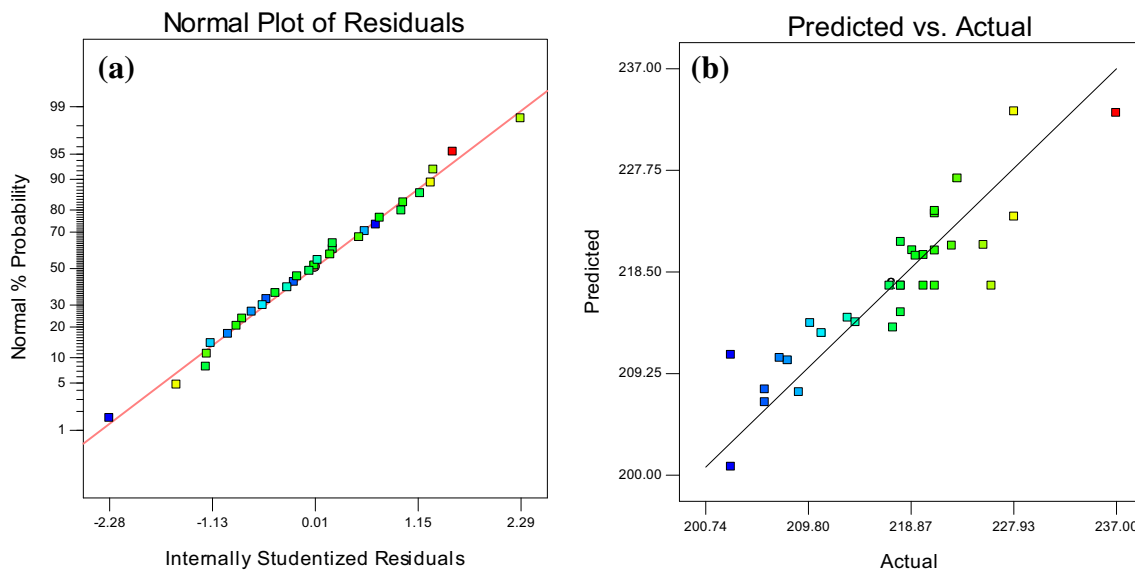


Fig. 4 **a** Normal probability plot of residuals and **b** plot of predicted response vs. actual value for the hardness of HAZ area

$$\begin{aligned}
 \text{HAZ Area} = & 527.55 - 7.21 * A - 8.67 * B + 5.40 * C \\
 & - 1.89 * D - 10.69 * E - 0.249 * A * B \\
 & + 0.054 * A * D + 0.37 * A * E + 0.11 \\
 & * B * E - 0.15 * C * E + 0.16 * B^2 \\
 & + 0.0006 * D^2
 \end{aligned} \quad (10)$$

$$\begin{aligned}
 \text{HAZ Hardness} = & + 481.55 - 1.70 * A - 6.31 * B \\
 & - 5.93 * C - 0.052 * D + 0.69 * E \\
 & + 0.17 * C * E + 0.099 * B^2 - 0.102 \\
 & * E^2
 \end{aligned} \quad (11)$$

3.2 Direct and interaction effects

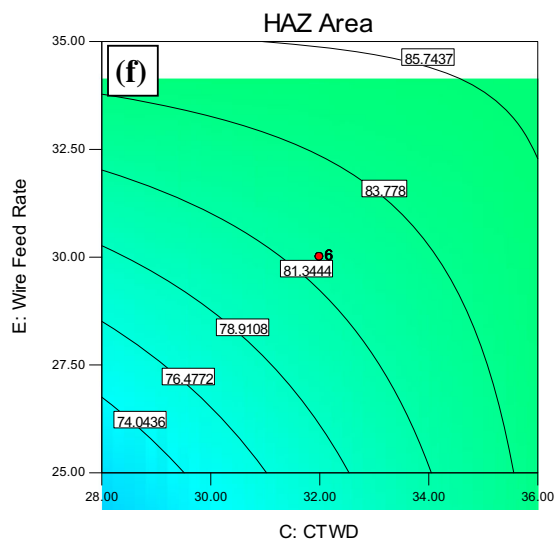
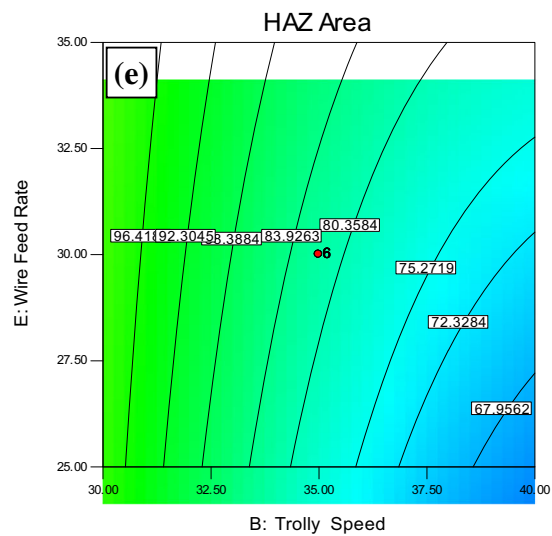
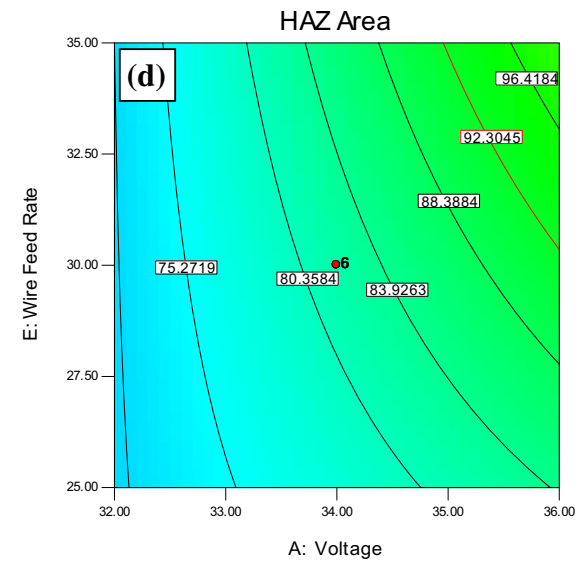
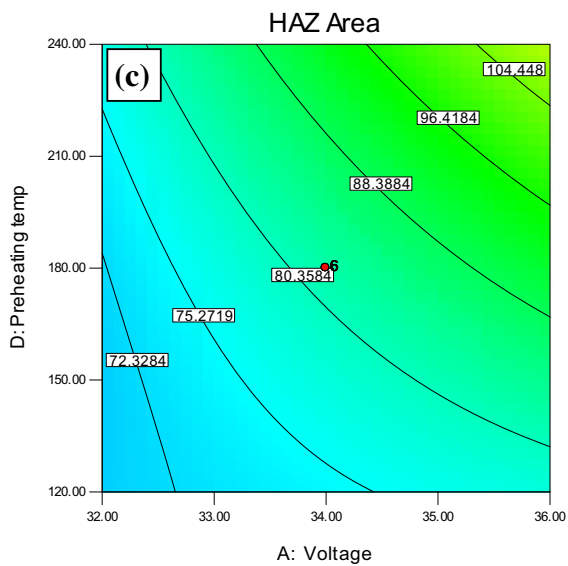
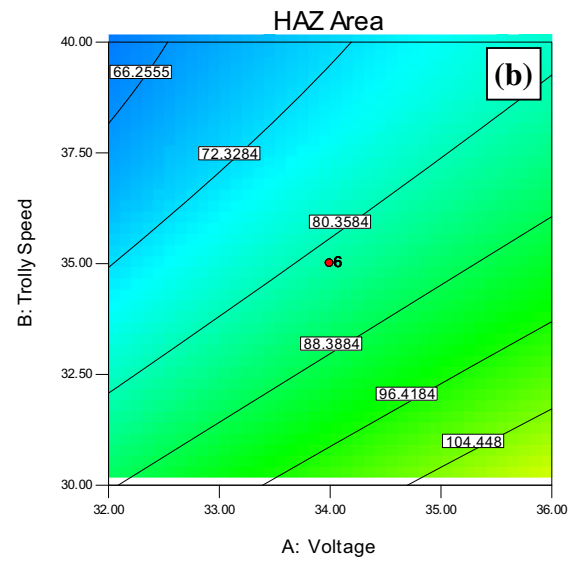
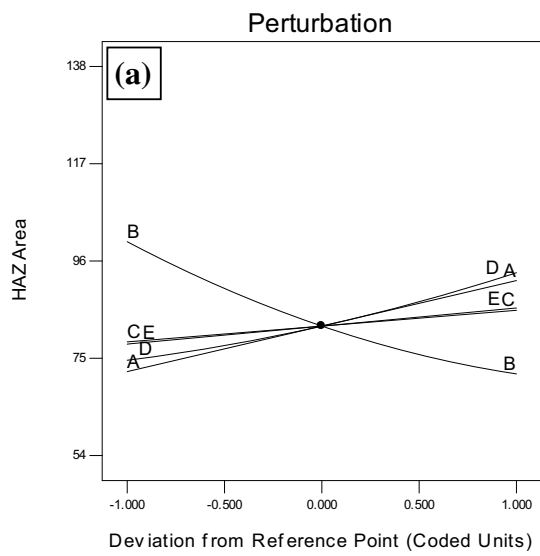
A perturbation plot provides the silhouette view of the response surface. Perturbation plot of SAW machine parameters and preheating temperature for HAZ area and HAZ hardness of X80 steel weld is shown in Figs. 5a and 6a, respectively. Perturbation plot shows the change in process response while each SAW process variable moves from the centre point while all other variables are kept constant at the centre value. Effects of significant interaction amid any two process parameters on HAZ area and HAZ hardness are illustrated in terms of contour plots in Figs. 5b–f and 6b, respectively. Contour plots are the graphical illustration of the relationships between three variables in two dimensions.

3.2.1 Effect of SAW process parameters on HAZ area

Figure 5a shows that the increase in voltage, contact tube to work distance, wire feed rate and preheating temperature

Fig. 5 **a** Perturbation plot showing the direct effect and **(b–f)** counterplots presenting the interaction effect of process variables on the HAZ area

results in increase of HAZ area while with an increase of welding speed, HAZ area decreases. This is because, higher values of voltage and contact tube to work distance increases the heat input of welding process. As in this machine, a constant voltage power source is used, so current adjusts accordingly as wire feed rate changes. This increase in current due to increase of wire feed rate also increases the welding heat. With the increase of preheating temperature, additional heat energy directly adds in heat input at workpiece. Hence, preheat also lowers the thermal gradient between two sections of the welded plate which gives slow cooling rate and high heat retention for a longer time. Welding speed denotes the speed of welding arc by which it moves over the plates or groove to be welded. Lower welding speed gives more time to the welding arc to remain at a point during welding and so the higher amount of heat is delivered to the plate per unit length. In addition to widening of HAZ, the higher heat input of welding process also promotes coarsening of grains in the HAZ. Lower heat input of welding gives insufficient heat for complete penetration as well as proper fusion of base plates and filler wire. Heat input of welding process also affects the metal transfer characteristics of welding arc, thus delivering heat to the base plates. With the increase of heat input, mode of metal transfer varies from globular transfer to a more fine spray transfer. From the understanding of direct effect of process parameters, their interaction effects (as shown in Fig. 5b–f) can also be understood accordingly.



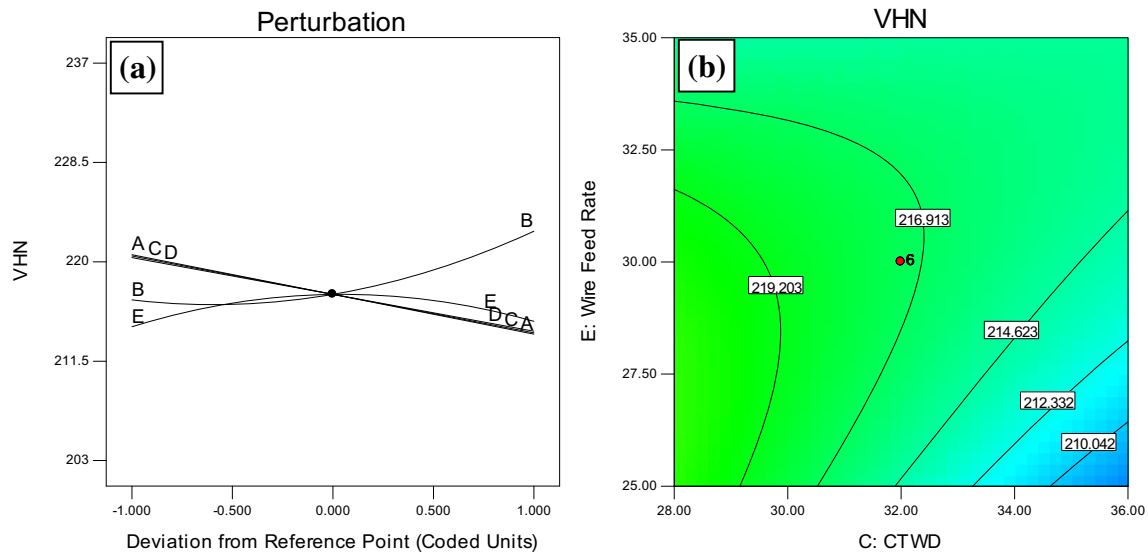


Fig. 6 **a** Perturbation plot showing the direct effect of all variables and **b** counterplot presenting the interaction effect of wire feed rate and contact tube to work distance (CTWD) on the hardness of HAZ area

3.2.2 Effect of SAW process parameters on hardness of HAZ

Figure 6a shows that the increase in voltage, contact tube to work distance and preheating temperature results in the decrease of HAZ hardness while with an increase of welding speed, the value of HAZ hardness increases. This is because, higher values of voltage and contact tube to work distance and lower value of welding speed of welding gun increases the heat input of welding process. With high heat input of the process, the cooling rate in HAZ region is slow which promotes a martensite-free microstructure. A higher value of preheating temperature also slows down the cooling rate of welding structure. With the increase in preheating temperature, additional heat energy directly adds up in heat input at workpiece which retains it for a longer time period. Wire feed rate has insignificant effect on HAZ hardness. At the start there is an increase in wire feed rate, hardness of HAZ microstructure increases but with further increase in wire feed rate, hardness value decreases. As in a constant voltage DC power source, welding current adjusts itself according to wire feed rate change. The increase of wire feed rate at the start, experiences an increase in heat energy due to increase in the value of welding current which is used in melting the extra wire feed. After a limit, more heat reaches the molten pool and the metal plate increases its heat input giving a less harder microstructure. Counterplot in Fig. 6b shows the effect of interaction amid contact tube to work distance and wire feed rate on HAZ hardness.

3.3 Relationship of heat input and cooling time with HAZ characteristics

Figure 7 depicts the relationship of HAZ characteristics with heat input and critical cooling time of welding. HAZ area is found to increase with increase of the heat input at a very steep rate as shown in Fig. 7a. It happens because at higher heat input, the current density reaches high due to higher wire feed rate. This increases the available energy of the arc at higher temperature. This energy at higher temperature remains in the weld for a comparatively longer time. Dissipation of this heat to the surrounding area also affects its microstructure. However, average hardness of the HAZ area has shown a decreasing trend with the increase of welding heat as clearly evident in Fig. 7b. This may happen because of the refinement in the microstructure occurring due to the high heat thermal cycles of welding.

In Fig. 7c, a linear increase in HAZ area with the increase of $\Delta t_{8/5}$ is clearly visible. This happens because the higher value of heat input as well as preheating temperature yields a higher $\Delta t_{8/5}$. Both at higher levels give more time to the thermal energy to dissipate from the weld as well as its adjacent area. Their higher values decrease the thermal gradient between two sections of the plate, and hence longer cooling time results in the higher area of HAZ. Opposite to the area of HAZ, its hardness is found to decrease with the increase of the critical cooling rate as evident in Fig. 7d. It occurs because at larger cooling time or slower cooling rate, changes occur in the microstructure uniformly which produce a pearlite or bainitic structure in

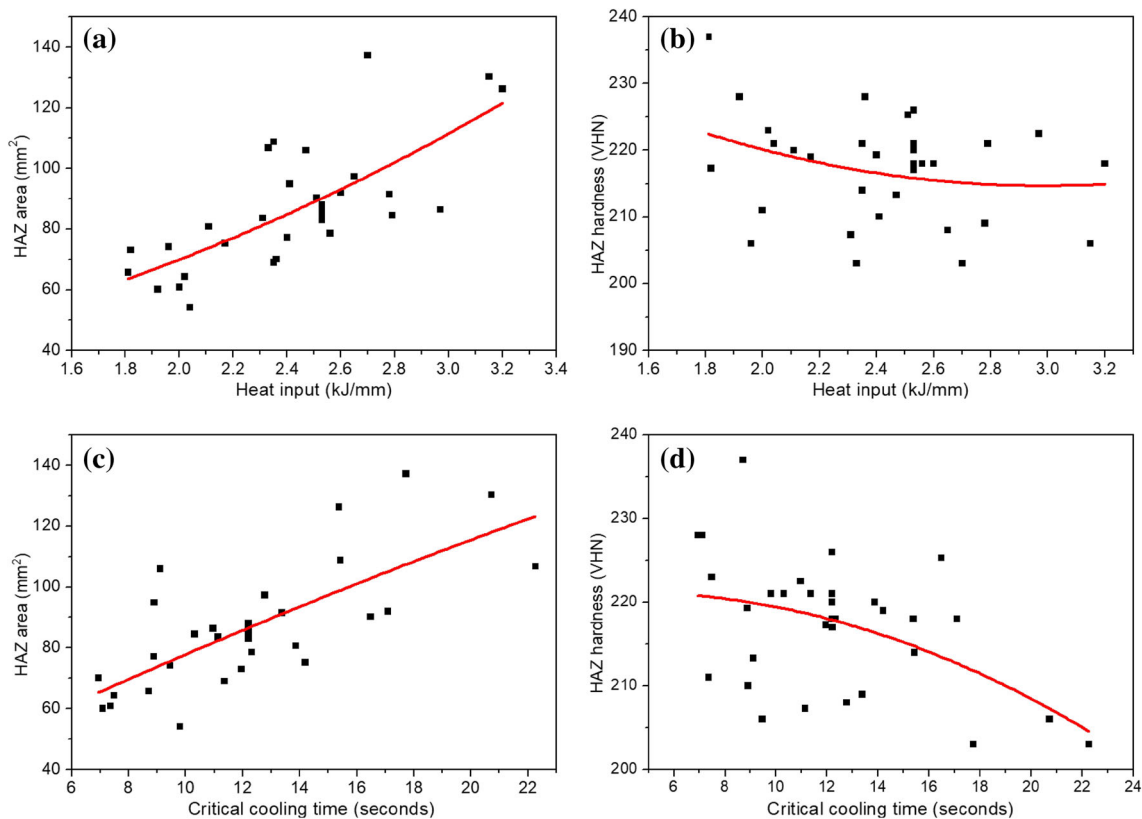
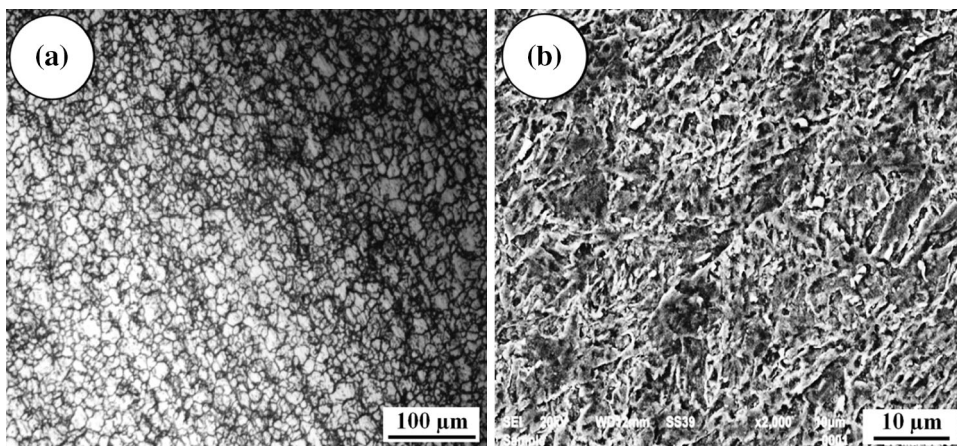


Fig. 7 Relationship of heat input vs. **a** HAZ area, **b** HAZ hardness and critical cooling time of weld vs. **c** HAZ area, **d** HAZ hardness

Fig. 8 **a** Optical micrograph and **b** scanning electron micrograph of parent metal structure



the HAZ which is comparatively more ductile as compared to the martensite structure produced in the weld with higher cooling rate or lesser cooling time.

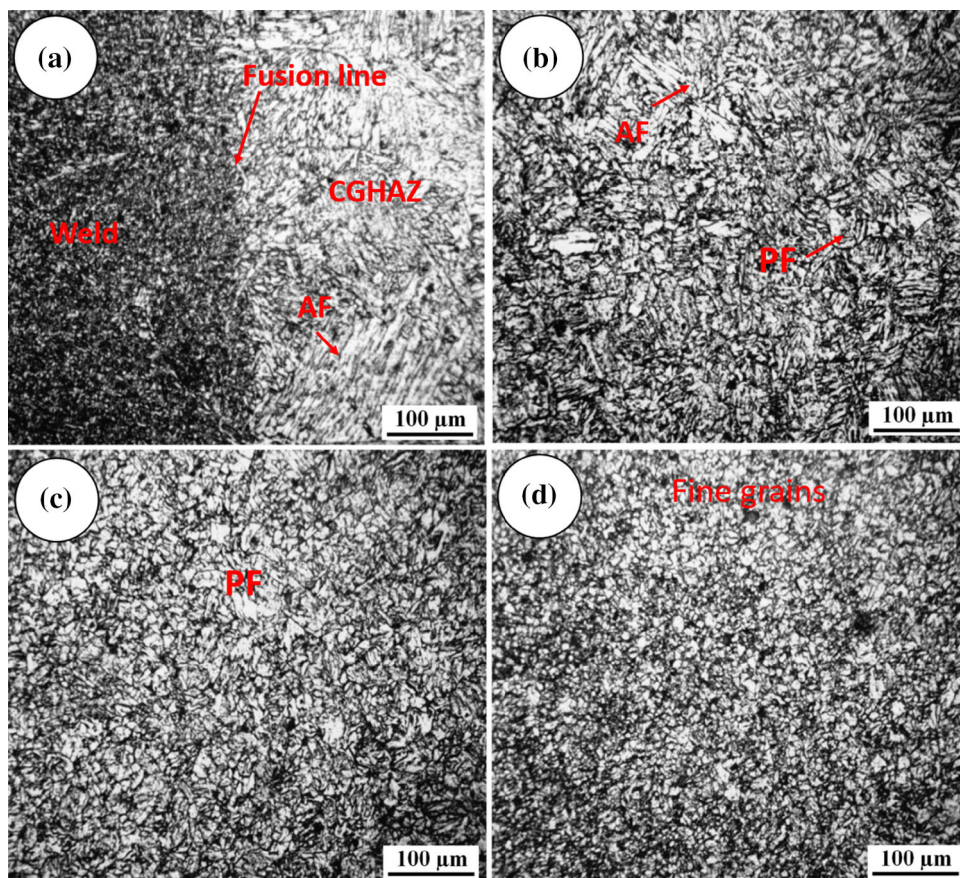
3.4 Microstructure analysis

3.4.1 Parent material

Microstructure of parent metal is investigated through optical as well as scanning electron microscope. These

micrographs (refer Fig. 8) clearly show the fine-grained microstructure of X80 steel consisting of polygonal ferrite (PF), quasi-polygonal ferrite and acicular ferrite (AF). This fine-grained structure of X80 steel helps to achieve high fracture toughness. A fine-grained structure is comparatively stronger and harder than a coarse-grained structure [29]. In fine-grained structure, larger amount of grain boundaries impede dislocation motion. Hall–Petch relation also supports this fact. From the optical analysis, grain size of parent material API X80 is found in the range of few

Fig. 9 For weld number 21, optical micrograph from **a** weld, fusion line and CGHAZ, **b** FGHAZ, **c** ICHAZ and **d** SCHAZ



micrometers (7–10 μm) only. Particles of second phase present in parent metal either as oxide inclusions, carbides or nitrides promote the formation of acicular ferrite microstructure and inhibit grain growth.

3.4.2 Welded area

The welding heat produces a thermal gradient between two portions of the joint. The steeper the thermal gradient between weld and unaffected portion of plate, the greater is the possibility of planar (columnar) growth. This happens because of the grains' tendency to solidify and grow in the direction which is perpendicular to the solid/liquid interface as in this direction maximum temperature gradient exists. Optical micrographs (Fig. 9) and scanning electron micrographs (Fig. 10) show these phenomena of grain growth and grain solidification across different sections of HAZ. As cooling time plays an important role in grain growth and microstructure development, grain size in different parts of welded joint is determined. Grain size is given in both, i.e., ASTM number and micron. Grain sizes in different parts of welded joint are tabulated in Table 6 for bead-on-plate experiments. Results of grains size measurement clearly support the role of cooling time in

grain growth. In welded joint, temperature varies from maximum at weld to gradually decreasing temperature across the fusion boundary, CGHAZ, FGHAZ, ICHAZ and minimum in SCHAZ. Higher critical cooling time produces a coarse microstructure while a fine microstructure is obtained with lower critical cooling time. This effect is uniform across all zones of welded area.

To distinguish the effect of thermal cycles on the different portions of welded joint, microstructure investigation is carried out starting from weld centre towards unaffected area of the plate. This covers weldment and different parts of the HAZ such as CGHAZ, FGHAZ, ICHAZ and SCHAZ. Figure 9 shows the optical micrographs of various portions of welded joint for experimental weld number 21. These micrographs clearly distinguish the fusion boundary and grain growth phenomena in the different subzones of HAZ. Microstructures developed in these different zones are also observed through scanning electron microscope. Scanning electron micrographs for different zones formed in weld number 21 are shown in Fig. 10. In the weld zone, developed microstructure mainly consists of acicular ferrite (Fig. 10a). In welded structures, acicular microstructure is always desired for higher fracture toughness. Acicular ferrite exhibits outstanding

Fig. 10 For weld number 21, scanning electron micrograph from **a** weld, **b** CGHAZ, **c** FGHAZ and **d** ICHAZ

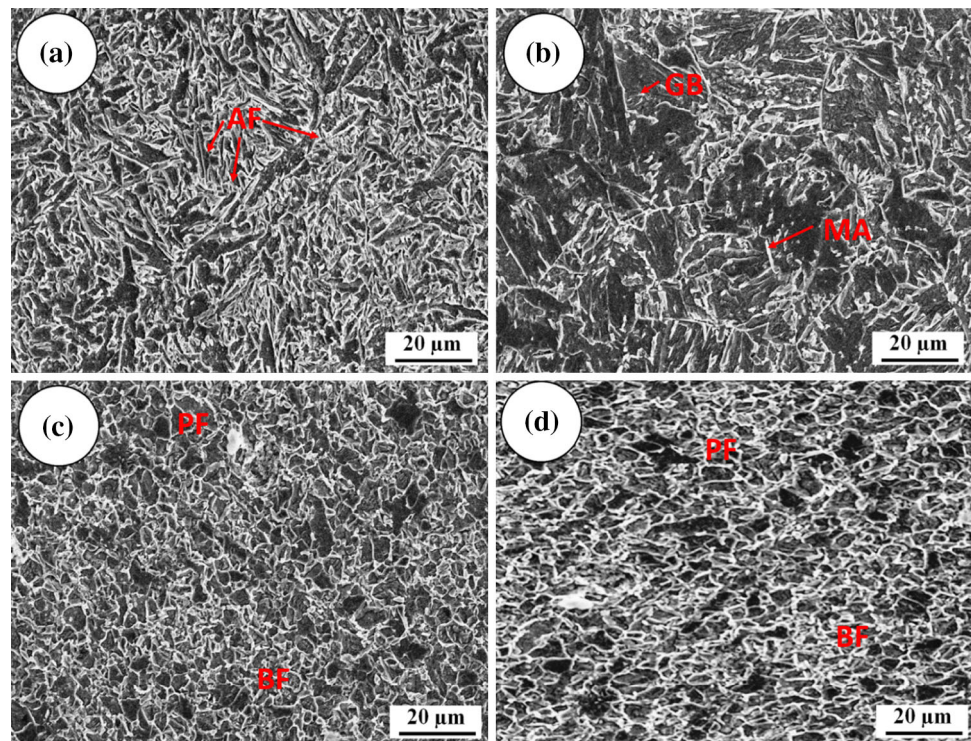


Table 6 Average grain size in different zones of bead-on-plate welds

Weld number	Critical cooling time (s)	Average grain size in ASTM number/ μm				
		Weld	CGHAZ	FGHAZ	ICHAZ	SCHAZ
15	15.38	8.6/16.3	4.7/63.4	8.3/18.0	9.3/12.7	10.0/10.0
17	22.26	7.1/22.7	3.8/86.0	7.7/21.5	8.3/18.0	9.4/12.3
20	10.31	9.4/12.3	5.0/56.6	9.0/14.1	9.5/11.9	9.9/10.4
21	06.94	9.8/10.8	6.5/33.6	9.5/11.9	9.8/10.8	10.5/8.4

combination of toughness and strength owing to its fine and irregularly shaped grains.

In CGHAZ, complete recrystallization and coarsening of grains have occurred as revealed in Fig. 10b. Microstructure in CGHAZ, where peak temperature generally reaches above 1200 °C [30] is found as a mixture of acicular ferrite and granular bainite along with M-A micro-constituents. As evident from Fig. 10c, microstructure in FGHAZ is a mixture of fine bainite, polygonal ferrite and little amount of M-A micro-constituents. With further decrease in peak temperature, the section produced between the upper and lower critical temperatures is ICHAZ. Microstructure developed in ICHAZ is found as mixture of bainite and quasi-polygonal ferrite along with micro-constituents (Fig. 10d). In SCHAZ, peak temperature remains under the lower critical temperature limit; therefore, only tempering occurs as transformation is not possible in this range of temperature. Hence, microstructure obtained in SCHAZ is formed of tempered bainite and ferrite.

3.5 Hardness profile across weld bead

Hardness in a section is the result of cooling rate experienced by that particular section during welding which is finally a function of heat input and preheating temperature. Therefore, over the whole range of critical cooling time (6.94–22.26 s) of conducted experiments (refer Table 3), hardness profile in four welds (9 ($\Delta t_{8/5} = 12.22$ s), 15 ($\Delta t_{8/5} = 15.38$ s), 17 ($\Delta t_{8/5} = 22.26$ s) and 21 ($\Delta t_{8/5} = 6.94$ s)) is presented. Hardness profile in these four welds is measured in bead-on-plate welds and presented in Fig. 11 in terms of VHN.

From Fig. 11, it is clear that microhardness value in HAZ is lower than the weld metal. It is because of the acicular ferritic microstructure of weld metal as compared to regular structure of HAZ. Hardness gradient across HAZ typically shows a maximum hardness immediately adjacent to the fusion boundary (where structure is a mixture of acicular ferrite and granular bainite along with M-A micro-

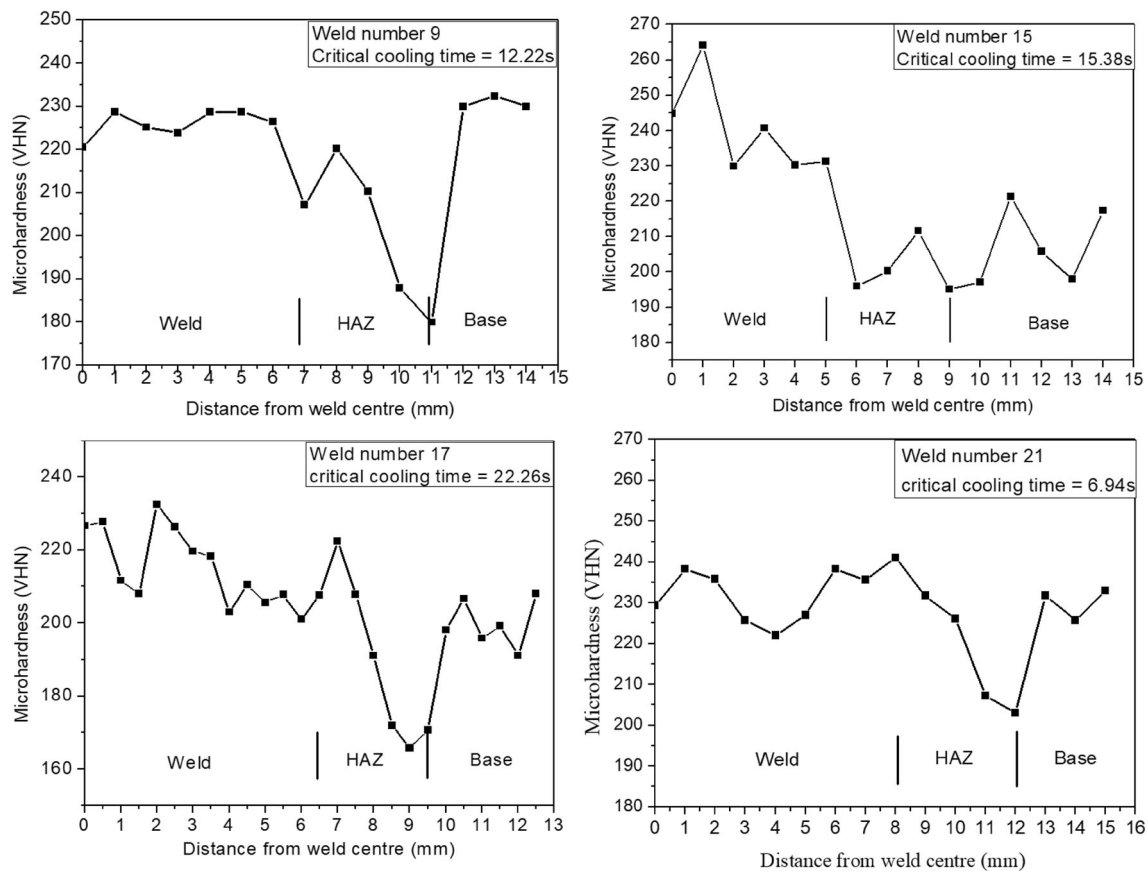


Fig. 11 Hardness profile in bead-on-plate welds

constituents) with a progressive decrease across CGHAZ, little increase in FGHAZ and again decrease across intercritically heated HAZ (ICHAZ). The initial decrease of hardness in CGHAZ is because of its coarser granular structure. This rise in hardness value across FGHAZ is due to its fine microstructure consisting of fine bainite, polygonal ferrite and little amount of M-A micro-constituents. A sharp decrease in hardness value in last region of HAZ is also observed. According to the literature, this sharp decrease of hardness value occurs across ICHAZ and subcritically heated HAZ (SCHAZ) [13]. In ICHAZ region, structure obtained is the mixture of bainite and quasi-polygonal ferrite which shows lower hardness as compared to base material. In SCHAZ region, softening of bainite and ferrite structure due to tempering is observed. It happens because peak temperature reaches up to lower critical temperature in SCHAZ during welding.

The actual form of the hardness gradient across base metal, HAZ and weld metal depends on the welding conditions and filler material used. In preparation of these welds, the same filler material is used, and therefore, it is the welding process parameters which control the hardness gradient. In weld numbers 15 and 17 where critical cooling times are 15.38 and 22.26 s, respectively, it is found that

hardness in weld metal is more than base material. This happens because of slow cooling of weld and formation of coarse bainite microstructure in it. On the other hand, in weld numbers 9 and 21 where critical cooling times are 12.22 and 6.94 s, respectively (comparatively lower heat input and faster cooling), the hardness of weld matches with hardness of base material. Lower amount of welding heat gives faster cooling to the weld material, and hence a fine-grained microstructure is obtained in the weld metal which shows strength and hardness comparatively similar to the fine-grained base material.

3.6 Results of desirability approach

3.6.1 Single-characteristic optimization

Constraints for the optimization of individual HAZ characteristic are defined in terms of goals and limits. Goals and limits for each variable help in determining its impact on individual desirability [31]. A goal of minimization is provided for HAZ area and HAZ hardness. Input parameters of SAW process are kept in their range as shown in Table 2. Weight of default value 1 is assigned to each goal to avoid any biasing in results. Actually, shape of the

Table 7 Optimized process parameters of SAW using desirability for area and hardness of HAZ

Purpose	A	B	C	D	E	HAZ hardness	HAZ Area	Desirability
Area minimum	37.71	38.77	32.18	64.95	24.87	–	41.73	1
Hardness minimum	36.09	38.83	36.94	254.3	20.28	191.17	–	1
Both minimum	37.35	40.73	37.20	113.60	21.28	201.50	50.83	1

desirability function for a goal is decided and controlled by its weight. For equal importance of each goal, an importance value of 3 is selected for each goal. Results for single-characteristic optimization using desirability approach are given in Table 7. This table contains the suggested values of input parameters which result in unit value of desirability for each goal.

3.6.2 Multi-characteristic optimization

Multi-characteristic optimization overcomes the problem of contradictory responses of single-characteristic optimization. As a single problem, HAZ area minimization and HAZ hardness minimization are provided as a goal with equal weight and equal importance. Input parameters are kept within their ranges similar to single-characteristic optimization problem. Suggested values of input parameters which yield a unit value of desirability for this goal are tabulated in Table 7.

3.7 Confirmatory experimentation

Verification of the mathematical regression equations and the results of desirability approach used for single as well as multi-objective optimization are necessary to check the prediction accuracy of the same on the practical ground. As response values are predicted by desirability approach using mathematical regression equations only, hence, confirmatory experiments carried out at optimal settings of process parameters suggested by desirability approach will be tested for both, i.e., applicability of desirability approach and prediction accuracy of mathematical regression equations. Confirmatory experiments are carried out as per Table 8. Values of process parameters are kept close to their optimal suggested value, as it is not feasible on economic basis to set their exact value because of the

constraints of machine setup. Desirability values of results of confirmatory tests for each case, i.e., single-objective as well as multi-objective, are calculated. A percentage error for each response is also calculated by comparing their experimental values (in Table 8) with their corresponding predicted values (in Table 7). From the experimental values, nearly a 10% error is observed for each response in almost all confirmatory experiments. Error percentage is calculated as:

$$\text{Error (\%)} = \frac{\text{actual value} - \text{predicted value}}{\text{predicted value}} \times 100$$

4 Conclusion

Using multiple regression analysis, for prediction purpose, modeling for HAZ area as well as its hardness has been carried out in relation to SAW process parameters and preheating temperature for their given ranges. A detailed microstructural analysis is also carried out across the different zones of the weld. Additionally, optimization of process parameters is carried out using desirability function approach. On the basis of the study findings, the following conclusions are drawn:

1. For the smaller area of HAZ which is always desired, the lower values of heat input or voltage, contact tube to work distance, preheating temperature, wire feed rate and higher value of welding speed are suggested. Similarly, for lower values of hardness in HAZ area, higher values of voltage, contact tube to work distance and preheating temperature and lower value of welding speed are suggested. The effect of wire feed rate on HAZ hardness is found as insignificant.
2. HAZ area is found to be increasing at a very steep rate with increase in heat input. It can happen because at higher heat input, available energy of the arc at higher temperature is high. Average hardness of the HAZ has

Table 8 Results of confirmatory experiments at optimized settings of process parameters

Purpose	A	B	C	D	E	Actual results		Desirability	Age variation (%)
						HAZ hardness	HAZ Area		
Area minimum	38	39	32	65	25	–	44.80	1	7.36
Hardness minimum	36	39	37	254	20	198	–	1	3.57
Both minimum (multi-objective)	37	41	37	114	21	206	55.84	0.95	2.23; 9.86

shown a decreasing trend with the increase of welding heat. This happens because of the refinement in the microstructure occurring due to the high heat thermal cycles of welding.

3. A linear increase in HAZ area with the increase of $\Delta t_{8/5}$ is observed. This happens because the higher value of heat input as well as preheating temperature yields a higher $\Delta t_{8/5}$. Opposite to the area of HAZ, its hardness is found to be decreasing with the increase of the critical cooling rate.
4. Results of the confirmatory experiments carried out at optimal settings of process parameters as suggested by the desirability approach for single as well as multi-characteristic optimization are found within $\pm 10\%$ of predicted values of HAZ characteristics. This proves the worthiness of the approach for optimization of SAW process parameters.
5. In the weld zone, developed microstructure mainly consists of acicular ferrite. It is always desirable to have acicular structure in weld as it exhibits outstanding combination of toughness and strength owing to its fine and irregularly shaped grains.
6. Optical as well as scanning electron microscopic analysis clearly prove that welding heat plays significant role in deciding the microstructure in weld and its adjacent area. As, welding heat produces a thermal gradient between two portions of the joint, therefore, grains tend to solidify and grow in the direction of maximum temperature gradient.

References

1. Sharma S K and Maheshwari S *J Mech Sci Technol* **31** (2017) 1383. <https://doi.org/10.1007/s12206-017-0238-6>.
2. American Petroleum Institute *API Specification 5L*, 45th Edition, API Publishing Services, Washington DC (2012).
3. Houldcroft P T *Submerged-Arc Welding* (Second Edition), Woodhead Publishing, Sawston (1989).
4. Sharma S K and Maheshwari S *J Nat Gas Sci Eng* **38** (2017) 203. <https://doi.org/10.1016/j.jngse.2016.12.039>.
5. Wang B, Xu Y, Hu J, Zhang s, Cui C, Lan H *Trans Indian Inst Met* (2018) <https://doi.org/10.1007/s12666-018-1382-0>.
6. Yin L, Wang J, Chen X, Liu C, Siddiquee A N, Wang G, Yao Z *Weld World* (2018). <https://doi.org/10.1007/s40194-018-0582-x>.
7. Zhang T, Zhao W, Deng Q and Jiang W *Int J Hydrogen Energy* **42** (2017) 25102. <https://doi.org/10.1016/j.ijhydene.2017.08.081>.
8. Sharma L and Chhibber R *Int J Press Vessel Pip* **165** (2018) 193. <https://doi.org/10.1016/j.ijpvp.2018.06.013>.
9. Yang M, Liu Y, Zhang, Xiang D *Trans Indian Inst Met* (2018). <https://doi.org/10.1007/s12666-018-1379-8>.
10. Poorhaydari K, Patchett B M and Ivey D G *Weld J* **84** (2005) 149–s.
11. Gunaraj V and Murugan N *Weld J* **81** (2002) 45–s.
12. Gunaraj V and Murugan N *J Mater Process Technol* **95** (1999) 246.
13. Jindal S, Chhibber R and Mehta N P *Proc IMechE Part B J Eng Manuf* **228** (2015) 82. <https://doi.org/10.1177/0954405413495846>.
14. Kiran D V, Basu B and De A *J Mater Process Technol* **212** (2012) 2041. <https://doi.org/10.1016/j.jmatprotec.2012.05.008>.
15. Adak D K, Mukherjee M and Pal T K *Trans Indian Inst Met* **68** (2015) 839. <https://doi.org/10.1007/s12666-015-0518-8>.
16. Joshi J R, Potta M, Adepu K, Katta R K, Gankidi MR *Trans Indian Inst Met* **70** (2017) 69. <https://doi.org/10.1007/s12666-016-0861-4>.
17. Saha A and Mondal S C *Trans Indian Inst Met* **70** (2017) 1491. <https://doi.org/10.1007/s12666-016-0945-1>.
18. Kruglova A A, Orlov V V and Sharapova D M *Metallurgist* **58** (2015) 806. <https://doi.org/10.1007/s11015-015-9999-2>.
19. Kumar S and Nath S K *Trans Indian Inst Met* **70** (2017) 239. <https://doi.org/10.1007/s12666-016-0880-1>.
20. Li L, Wang Y, Han T and Li C *Int J Miner Metall Mater* **18** (2011) 419. <https://doi.org/10.1007/s12613-011-0456-3>.
21. Permyakov I L, Frantov I I, Bortsov A N and Mentuykov K Y *Metallurgist* **55** (2012) 925. <https://doi.org/10.1007/s11015-012-9523-x>.
22. Li H, Liang J-L, Feng Y-L and Huo D-X *Rare Met* **33** (2014) 493. <https://doi.org/10.1007/s12598-014-0344-x>.
23. Yang J R, Lion S H *Sci Technol Weld Join* **2** (1997) 119. <https://doi.org/10.1179/stw.1997.2.3.119>.
24. DuPont J N, Marder A R *Welding Res Supplement*, December (1995) 406s–416s.
25. Easterling K E (1992) *Introduction to the physical metallurgy of welding*, Butterworth Heinemann, Oxford.
26. Montgomery D C *Design and analysis of experiments*, Wiley, New York (2013).
27. Sharma S K, Maheshwari S and Rathee S *J Manuf Sci Prod* **16** (2016) 141. <https://doi.org/10.1515/jmsp-2016-0009>.
28. Derringer G and Suich R *J Qual Technol* **12** (1980) 214.
29. Yee S V, Hussain Z, Anasyida AS, Syukron M, Almanar I P *Adv Mater Res* **858** (2013) 3. <https://doi.org/10.4028/www.scientific.net/amr.858.3>.
30. Saini N, Pandey C and Mahapatra M M *Trans Indian Inst Met* **70** (2017) 1. <https://doi.org/10.1007/s12666-017-1145-3>.
31. Kumar H, Manna A and Kumar R *Trans Indian Inst Met* **71** (2018) 231. <https://doi.org/10.1007/s12666-017-1159-x>.